

An ILUES-based adaptive Gaussian process method for multimodal Bayesian inverse problems

Zhihang Xu^{a,1}, Xiaoyu Zhu^{b,1}, Daoji Li^c, Qifeng Liao^{b,*}

^a*Department of Mathematics, University of Houston, Houston 77204, USA*

^b*School of Information Science and Technology, ShanghaiTech University, Shanghai 201210, China*

^c*Department of Information Systems and Decision Sciences, California State University, Fullerton 92831, USA*

Abstract

Inverse problems are prevalent in both scientific research and engineering applications. In the context of Bayesian inverse problems, sampling from the posterior distribution can be particularly challenging when the forward models are computationally expensive. This challenge is further compounded when the posterior distribution is multimodal. To address this issue, we propose a Gaussian process (GP)-based method to indirectly build surrogates for the forward model. Specifically, the unnormalized posterior density is expressed as a product of an auxiliary density and an exponential GP surrogate. Iteratively, the auxiliary density converges to the posterior distribution, starting from an arbitrary initial density. However, the efficiency of GP regression is highly influenced by the quality of the training data. Therefore, we utilize the iterative local updating ensemble smoother (ILUES) to generate high-quality samples that are concentrated in regions with high posterior probability. Subsequently, based on the surrogate model and mode information extracted using a clustering method, Markov chain Monte Carlo (MCMC) with a Gaussian mixed (GM) proposal is used to draw samples from the auxiliary density. Through numerical examples, we demonstrate that the proposed method can accurately and efficiently represent the posterior with a limited number of forward simulations.

Keywords: Bayesian inverse problems, Multimodal, Gaussian process, Surrogate, ILUES

1. Introduction

Inverse problems have a wide range of applications across many fields in science and engineering, such as weather prediction, groundwater flows, medicine, and molecular dynamics [1, 2, 3, 4]. Inverse problems typically involve learning the inputs to a mathematical model, such as physical parameters and initial conditions, based on partial and noisy observations of model outputs. Bayesian inverse problems (BIPs) provide a rigorous foundation to quantify uncertainty in the inverse solution [5]. BIPs capture the uncertainty associated with parameters by incorporating prior knowledge about the model inputs into a probability distribution, known as the prior distribution. By conditioning the prior distribution on the observed data, a posterior distribution is generated, providing a more accurate representation

*Corresponding author

Email addresses: zxu29@central.uh.edu (Zhihang Xu), zhuxiaoyu@sinopeda.com (Xiaoyu Zhu), dali@fullerton.edu (Daoji Li), liaoqf@shanghaitech.edu.cn (Qifeng Liao)

¹These authors contributed equally to this work.

of the model inputs. However, forward models, which map the parameters to measurable data in inverse problems, are often computationally expensive and complex when involving partial differential equations.

In many applications, the posterior distribution does not have a closed-form expression and must be approximated. In such cases, Markov Chain Monte Carlo (MCMC) is commonly used as a powerful method for exploring the posterior distribution [6, 7, 8, 9, 10, 11]. The standard MCMC method consists of three steps in each iteration: (i) generating a candidate sample from the proposal distribution, (ii) computing the acceptance probability, and (iii) either accepting or rejecting the candidate sample. Through repeated iterations, the distribution of the generated samples ultimately converges to the posterior distribution. However, when forward model evaluations are costly and the posterior distribution is multimodal, two main challenges arise for the standard MCMC approach. First, due to the Markov chain navigating low-probability barriers between modes, the MCMC sampler frequently becomes trapped within a single mode. Second, since MCMC methods require solving the forward model for every sample, the computational cost of MCMC simulations can become prohibitively high. To address these challenges, several variants of the standard MCMC approach have been proposed to enhance its performance in handling multimodal posterior distributions. One notable variant is parallel tempering (PT), also known as replica exchange Monte Carlo, which runs multiple Markov chains in parallel with each chain exploring the target distribution at a different “temperature” and swaps states between any two chains at intervals [12, 13, 14]. Another variant is the Differential Evolution Adaptive Metropolis (DREAM) algorithm, which combines the strengths of differential evolution and the Metropolis-Hastings algorithm. It has been widely used in inverse problems involving multimodal distributions and high-dimensional inputs [15, 16, 17]. The key idea behind these variants for sampling multimodal distributions is to sufficiently explore the parameter space. However, these variants typically require more simulations than the standard MCMC.

When dealing with a computationally expensive forward model, an effective strategy is to develop a computationally inexpensive surrogate model, which can replace the original forward model for tasks such as calculating acceptance probabilities, parameter estimation, and uncertainty quantification. Some popular surrogate models in BIPs include Gaussian process regression [18, 19, 20], polynomial chaos expansion [21, 22, 23], deep neural networks [24, 25], and local approximation [26, 27, 28]. These surrogate models approximate the true forward model by using a training set of input-output pairs. A good strategy for selecting the training set is to choose data points from the high-density regions of the posterior distribution [29, 30]. However, identifying the high-density regions of a multimodal posterior distribution is a challenging task. Moreover, for BIPs with multimodal posterior distributions, the combination of MCMC sampling and surrogate methods can lead to unsatisfactory results.

The ensemble Kalman filter (EnKF), widely used in dynamical systems, is a derivative-free optimizer that selects samples to approximate a target distribution, which is typically assumed to be Gaussian. The ensemble smoother (ES), a variant of EnKF, updates the samples utilizing all available data, leading to reduced computational costs [31, 32, 33]. Both EnKF and ES can provide reliable estimates of the parameter of interest when a sufficiently large ensemble size is used. However, due to the computationally intensive nature of the forward model, only a small ensemble is feasible. Furthermore, EnKF and ES inherently provide a unimodal Gaussian approximation to the posterior distribution, which may fail to capture the complexities of the true distribution, particularly when the posterior is multimodal. To address

these issues, the iterative local updating ensemble smoother (ILUES) was proposed. Its main idea is to iteratively update localized regions within the ensemble [34]. One of the appealing properties of ILUES is its ability to concentrate the ensemble samples in regions with high posterior density.

In this paper, we propose an adaptive approximation sampler for multimodal posterior distributions by combining the adaptive Gaussian process (GP) framework and the ILUES method. Specifically, the proposed approach consists of three main steps. First, we express the unnormalized posterior density as the product of an auxiliary density and the exponential of the target function, which is approximated using a GP surrogate. The training data of the GP surrogate are selected using the ILUES method since ILUES-generated samples can quickly accumulate in regions of high posterior density. Next, we divide these ILUES-generated samples into K clusters using the K -means method and obtain preliminary cluster information, including the number of clusters, as well as the mean and covariance of each cluster. Finally, we sample from the approximated posterior distribution using MCMC, with the proposal distribution being a Gaussian mixture whose parameters are derived from the final iteration of the ILUES method.

The rest of the paper is organized as follows. Section 2 introduces the formulation of Bayesian inverse problems. Section 3 provides a brief review of the adaptive Gaussian process surrogate and the ILUES method. Section 4 presents the proposed approach for approximating multimodal posterior distributions. Section 5 demonstrates the performance of the proposed method through numerical examples. Section 6 concludes the paper.

2. Bayesian inverse problems

In a Bayesian inverse problem, we seek to estimate a parameter vector $\theta \in \Theta \subseteq \mathbb{R}^{\bar{M}}$ based on observed data $\mathbf{d}_{obs} \in \mathbb{R}^{\bar{D}}$, where \bar{M} is the dimension of the parameter space and \bar{D} is the dimension of the data space. The forward model is typically defined as a function $\mathcal{G} : \mathbb{R}^{\bar{M}} \rightarrow \mathbb{R}^{\bar{D}}$. The relationship between θ and \mathbf{d}_{obs} is described by

$$\mathbf{d}_{obs} = \mathcal{G}(\theta) + \eta,$$

where η represents the measurement noise. Using Bayes' theorem, the posterior probability density of θ given \mathbf{d}_{obs} is given by

$$\pi(\theta|\mathbf{d}_{obs}) = \frac{\mathcal{L}(\mathbf{d}_{obs}|\theta)\pi_{prior}(\theta)}{\int \mathcal{L}(\mathbf{d}_{obs}|\theta)\pi_{prior}(\theta)d\theta} \propto \mathcal{L}(\mathbf{d}_{obs}|\theta)\pi_{prior}(\theta).$$

Here $\mathcal{L}(\mathbf{d}_{obs}|\theta)$ is the likelihood and $\pi_{prior}(\theta)$ is the prior, which reflects the initial knowledge of θ before observing the data. Under the assumption that η is a \bar{D} -dimensional zero mean Gaussian noise with the non-singular covariance matrix Σ_η , i.e., $\eta \sim \mathcal{N}(\mathbf{0}, \Sigma_\eta)$, the likelihood takes the following form

$$\mathcal{L}(\mathbf{d}_{obs}|\theta) \propto \exp\left\{-2^{-1} [\mathbf{d}_{obs} - \mathcal{G}(\theta)]^T \Sigma_\eta^{-1} [\mathbf{d}_{obs} - \mathcal{G}(\theta)]\right\}.$$

To get the uncertainty quantification of θ , a commonly used approach is to generate samples from the posterior distribution $\pi(\theta|\mathbf{d}_{obs})$. However, when the forward model $\mathcal{G}(\theta)$ is nonlinear in θ , the posterior $\pi(\theta|\mathbf{d}_{obs})$ does not admit a closed-form expression.

3. Overview of the adaptive GP surrogate and the ILUES method

3.1. Adaptive GP surrogate

Computing the log-likelihood function $\mathcal{L}(\mathbf{d}_{obs}|\theta)$ is often computationally expensive, as it requires repeated evaluations of the forward model. To address this challenge, a common approach is to employ Gaussian process regression to approximate the log-likelihood function. Let us briefly review the idea. Let the target function be $F(\theta)$, and suppose we have access to N data pairs, $\{(\theta_i, F(\theta_i))\}_{i=1}^N$. The GP surrogate model predicts $F(\theta^*)$, which is the value of the target function at any new point θ^* . The key idea of Gaussian process regression is to assume that the target function $F(\theta)$ is a realization of a Gaussian random field, characterized by a mean function $\mu(\theta)$ and a covariance function defined by a kernel $k(\theta, \theta')$, i.e., $F(\theta) \sim \mathcal{GP}(\mu(\theta), k(\theta, \theta'))$. Write $\mathbf{x} = [\theta_1, \dots, \theta_N]$ and $\mathbf{y} = [F(\theta_1), \dots, F(\theta_N)]$. Then the joint distribution of \mathbf{y} and $F(\theta^*)$ is

$$\begin{bmatrix} \mathbf{y} \\ F(\theta^*) \end{bmatrix} \sim \mathcal{N} \left(\begin{bmatrix} \mu(\mathbf{x}) \\ \mu(\theta^*) \end{bmatrix}, \begin{bmatrix} K(\mathbf{x}, \mathbf{x}) & K(\mathbf{x}, \theta^*) \\ K(\theta^*, \mathbf{x}) & k(\theta^*, \theta^*) \end{bmatrix} \right), \quad (1)$$

where $\mu(\mathbf{x})$ is an $N \times 1$ vector with the i -th element $\mu(\theta_i)$, $K(\mathbf{x}, \mathbf{x})$ is an $N \times N$ covariance matrix with the (i, j) entry $K_{ij} = k(\theta_i, \theta_j)$, $K(\mathbf{x}, \theta^*)$ is an $N \times 1$ vector with the i -th element $k(\theta_i, \theta^*)$, and $K(\theta^*, \mathbf{x})$ is the transpose of $K(\mathbf{x}, \theta^*)$. It follows from (1) that the posterior distribution of $F(\theta^*)$ is given by

$$\pi(F(\theta^*)|\mathbf{x}, \mathbf{y}, \theta^*) = \mathcal{N}(\tilde{\mu}(\theta^*), \text{var}(F(\theta^*))),$$

where the posterior mean and variance are

$$\tilde{\mu}(\theta^*) = \mu(\theta^*) + K(\theta^*, \mathbf{x})[K(\mathbf{x}, \mathbf{x})]^{-1}[\mathbf{y} - \mu(\mathbf{x})], \quad (2)$$

and

$$\text{var}(F(\theta^*)) = k(\theta^*, \theta^*) - K(\theta^*, \mathbf{x})[K(\mathbf{x}, \mathbf{x})]^{-1}K(\mathbf{x}, \theta^*), \quad (3)$$

respectively. Thus, we can use (2) to approximate $F(\theta^*)$ and (3) to quantify the approximation error, respectively.

However, when the log-likelihood function $\log \mathcal{L}(\mathbf{d}_{obs}|\theta)$ is highly nonlinear and complex, this approach may not provide accurate approximations [18]. To address this issue, [20] proposed an adaptive Gaussian process scheme. By Bayes' theorem, the unnormalized posterior probability density can be expressed as

$$\tilde{\pi}(\theta|\mathbf{d}_{obs}) = \mathcal{L}(\mathbf{d}_{obs}|\theta)\pi_{prior}(\theta) = \exp(f(\theta))p(\theta), \quad (4)$$

where $p(\theta)$ is an auxiliary distribution that can be freely chosen. According to (4), we set the target function as

$$f(\theta) = \log \left(\frac{\tilde{\pi}(\theta|\mathbf{d}_{obs})}{p(\theta)} \right). \quad (5)$$

In this formulation, the target function is smoothed by the logarithm, ensuring that the resulting posterior distribution, $\tilde{\pi}(\theta|\mathbf{d}_{obs})$, remains positive. It is also important to note that if the auxiliary distribution $p(\theta)$ provides a good approximation of the posterior, then $f(\theta)$ will be nearly constant and easier to approximate. Therefore, selecting an appropriate $p(\theta)$ can simplify the approximation process and enhance the accuracy of the model.

It is clear that the optimal choice for $p(\theta)$ would be the posterior distribution. However, this is impractical in the context of inverse problems. Therefore, starting with an initial density $p_0(\theta)$, an adaptive iterative framework is employed to refine $p(\theta)$, allowing it to converge to the posterior distribution $\pi(\theta|\mathbf{d}_{obs})$. The procedure proceeds as follows. Denote by $p_{n-1}(\theta)$ the current distribution at the n -th iteration. First, a Gaussian process model $\hat{f}_{n-1}(\theta)$ is constructed for $f_{n-1}(\theta)$, which is the log of the ratio between the posterior and the prior

$$f_{n-1}(\theta) := \log \left(\frac{\tilde{\pi}(\theta|\mathbf{d}_{obs})}{p_{n-1}(\theta)} \right). \quad (6)$$

Then, the GP surrogate $\hat{f}_{n-1}(\theta)$ is used to update $p_n(\theta)$ based on the approximation

$$p_n(\theta) \propto \exp(\hat{f}_{n-1}(\theta))p_{n-1}(\theta). \quad (7)$$

A detailed scheme can be found in Algorithm 1.

Algorithm 1 The adaptive GP algorithm

Input: Maximum number of iterations N^{\max} , KL divergence threshold δ_{KL} , maximum consecutive times N_{KL}^{\max} .

Output: The approximate posterior distribution $p_n(\theta)$.

- 1: Let $\hat{p}_0(\theta) = \pi_{prior}(\theta)$, $n_{KL} = 0$.
 - 2: Select m_0 initial design points $\theta_{i=1}^{m_0}$, and compute $y_i = f(\theta_i)$ for $i = 1, \dots, m_0$, with f defined in (5).
 - 3: Define the initial training data set as $S_0 = \{\theta_i, y_i := f(\theta_i)\}_{i=1}^{N_{m_0}}$.
 - 4: Construct an initial GP surrogate model $\hat{f}_0(\theta)$ for $f_0(\theta)$ (see (6)) using the data set S_0 .
 - 5: **for** $n = 1, \dots, N^{\max}$ **do**
 - 6: Draw N_m samples, denoted A_n , from the approximate posterior $p_n(\theta) \propto \exp(\hat{f}_{n-1}(\theta))\hat{p}_{n-1}(\theta)$ using MCMC.
 - 7: Obtain an estimated probability density function (PDF) \hat{p}_n from samples A_n .
 - 8: Compute $D_{KL}(\hat{p}_{n-1}(\theta), \hat{p}_n(\theta))$.
 - 9: **if** $D_{KL}(\hat{p}_{n-1}(\theta), \hat{p}_n(\theta)) < \delta_{KL}$ **then**
 - 10: $n_{KL} = n_{KL} + 1$.
 - 11: **else**
 - 12: Reset $n_{KL} = 0$.
 - 13: **end if**
 - 14: **if** $n_{KL} = N_{KL}^{\max}$ **then**
 - 15: Break the for loop.
 - 16: **end if**
 - 17: Choose m design points $\{\theta_i\}_{i=1}^m$ and compute $y_i = f(\theta_i)$ for $i = 1, \dots, m$ (f is defined in (5)).
 - 18: Enlarge the training data set as $S_n = S_{n-1} \cup \{(\theta_i, f(\theta_i))\}_{i=1}^m$.
 - 19: Construct the GP surrogate model $\hat{f}_n(\theta)$ with $\hat{p}_n(\theta)$ and the training data S_n
 - 20: **end for**
-

Termination can be triggered by either of two criteria. The first criterion is reaching the maximum number of iterations. The second criterion is based on the Kullback-Leibler (KL) divergence between p_{n-1} and p_n . If the $D_{KL}(p_{n-1}, p_n)$

is smaller than a specified threshold for N_{KL}^{max} consecutive iterations, it indicates that p_t has converged.

3.2. Iterative local updating ensemble smoother (ILUES)

As mentioned earlier, GP has its own limitations. Being a kernel-based method, the performance of GP approximation on test data heavily depends on the quality of the training data. In Algorithm 1, the selection of design points plays a crucial role in the effectiveness of the GP. Therefore, ILUES has been introduced as an efficient method for generating the training data. To present the ILUES method, let us first begin with the ensemble smoother. The ensemble smoother (ES) [33] is a fast and efficient method for the parameter estimation in nonlinear problems. For an ensemble of parameters $[\theta_1^t, \dots, \theta_{N_e}^t]$ at the t -iteration, where each $\theta_j^t \in \mathbb{R}^{\bar{M}}$, the ES updates the ensemble with

$$\theta_j^{t+1} = \theta_j^t + \Sigma_{\Theta\mathbf{D}}^t (\Sigma_{\mathbf{D}\mathbf{D}}^t + \Sigma_\eta)^{-1} (\tilde{\mathbf{d}}_j - \mathcal{G}(\theta_j^t)), \quad j = 1, 2, \dots, N_e$$

where N_e denotes the number of ensemble members and Σ_η is the covariance matrix of the measurement errors. The empirical covariances $\Sigma_{\Theta\mathbf{D}}^t$ and $\Sigma_{\mathbf{D}\mathbf{D}}^t$ are given by

$$\Sigma_{\Theta\mathbf{D}}^t = \frac{1}{N_e - 1} \sum_{i=1}^{N_e} (\theta_i^t - \bar{\theta}^t) \otimes (\mathcal{G}(\theta_i^t) - \bar{\mathcal{G}}^t) \quad \text{and} \quad \Sigma_{\mathbf{D}\mathbf{D}}^t = \frac{1}{N_e - 1} \sum_{i=1}^{N_e} (\mathcal{G}(\theta_i^t) - \bar{\mathcal{G}}^t) \otimes (\mathcal{G}(\theta_i^t) - \bar{\mathcal{G}}^t),$$

respectively, where the symbol \otimes denotes the Kronecker matrix product, $\bar{\theta}^t$ is the average of the ensemble $\{\theta_j^t\}_{j=1}^{N_e}$, and $\bar{\mathcal{G}}^t$ is the average of $\{\mathcal{G}(\theta_j^t)\}_{j=1}^{N_e}$.

Note that $\Sigma_{\Theta\mathbf{D}}^t$ is the $\bar{D} \times \bar{M}$ cross-covariance matrix between the parameter samples $\{\theta_j^t\}_{j=1}^{N_e}$ and the corresponding predicted data $\{\mathcal{G}(\theta_j^t)\}_{j=1}^{N_e}$, $\Sigma_{\mathbf{D}\mathbf{D}}^t$ is the $\bar{D} \times \bar{D}$ auto-covariance matrix of predicted data $\{\mathcal{G}(\theta_j^t)\}_{j=1}^{N_e}$, and $\tilde{\mathbf{d}}_j$ is the vector of observed data with $\tilde{\mathbf{d}}_j \sim \mathcal{N}(\mathbf{d}_j, \Sigma_\eta)$ where $\mathbf{d}_j = \mathcal{G}(\theta_j^t)$. It is clear from the update scheme of the ES that the method mainly depends on the mean and covariance information. Hence, when the posterior distribution is multimodal, ES would be unreliable. To address this, [34] proposed iterative local updating ensemble smoother (ILUES) algorithm, which extends ES to handle multimodal posterior distributions. Although the target distribution is multimodal, the local distribution remains unimodal. By leveraging this property, ILUES employs a local update strategy.

For $\theta \in \{\theta_j^t\}_{j=1}^{N_e}$, let

$$J(\theta) = J_1(\theta)/J_1^{max} + J_2(\theta)/J_2^{max} \quad (8)$$

be an integrated distance measure that accounts for both the discrepancy with the observed data \mathbf{d}_{obs} and the distance to the sample θ_j^t , where $J_1(\theta) = (\mathcal{G}(\theta) - \mathbf{d}_{obs})^T \Sigma_\eta^{-1} (\mathcal{G}(\theta) - \mathbf{d}_{obs})$ evaluates the discrepancy between the forward model $\mathcal{G}(\theta)$ and data \mathbf{d}_{obs} , and $J_2(\theta) = (\theta - \theta_j^t)^T \Sigma_{\Theta\Theta}^{-1} (\theta - \theta_j^t)$ quantifies the distance between the parameters θ and sample θ_j^t . Here, $\Sigma_{\Theta\Theta}$ denotes the $\bar{M} \times \bar{M}$ auto-covariance matrix of parameters θ . The normalization constants J_1^{max} and J_2^{max} are the maximum values of $J_1(\theta)$ and $J_2(\theta)$, respectively. The local ensemble associated with θ_j^t is then defined as the subset of N_l samples with the smallest values of $J(\theta)$, where $N_l = \alpha N_e$ and $0 < \alpha < 1$. This local ensemble is denoted by $\{\theta_{j,i}^t\}_{i=1}^{N_l}$. The ILUES update rule can therefore be expressed as

$$\theta_{j,i}^{t+1} = \theta_{j,i}^t + \Sigma_{\Theta\mathbf{D}}^{l,t} (\Sigma_{\mathbf{D}\mathbf{D}}^{l,t} + \Sigma_\eta)^{-1} (\tilde{\mathbf{d}}_i - \mathcal{G}(\theta_{j,i}^t)), \quad (9)$$

for $i = 1, 2, \dots, N_i$. Here, $\Sigma_{\text{OD}}^{l,t}$ is the $\bar{D} \times \bar{M}$ cross-covariance matrix between the local ensemble $\{\theta_{j,i}^t\}_{i=1}^{N_i}$ and the corresponding predicted data $\{\mathcal{G}(\theta_{j,i}^t)\}_{i=1}^{N_i}$, while $\Sigma_{\text{DD}}^{l,t}$ is the $\bar{D} \times \bar{D}$ auto-covariance matrix of predicted data $\{\mathcal{G}(\theta_{j,i}^t)\}_{i=1}^{N_i}$. Finally, a sample is randomly selected from $\{\theta_{j,i}^{t+1}\}_{i=1}^{N_i}$ to serve as the updated sample θ_j^{t+1} . The ILUES method is summarized in Algorithm 2.

Algorithm 2 Iterative local updating ensemble smoother (ILUES)

Input: Forward model $\mathcal{G}(\theta)$, observational data \mathbf{d}_{obs} , maximum number of iterations N_{iter} , ensemble size N_e .

Output: $\{\theta_j^{N_{\text{iter}}}\}_{j=1}^{N_e}$.

- 1: Sample $\{\theta_j^0\}_{j=1}^{N_e}$ from the prior distribution $\pi_{\text{prior}}(\theta)$ and calculate the predicted data $\{\mathcal{G}(\theta_j^0)\}_{j=1}^{N_e}$ correspondingly.
 - 2: **for** $t = 1 \cdots N_{\text{iter}}$ **do**
 - 3: **for** $j = 1 \cdots N_e$ **do**
 - 4: Calculate $J(\theta)$ for each $\theta \in \{\theta_j^t\}_{j=1}^{N_e}$ using (8).
 - 5: Calculate the updated local ensemble $\{\theta_{j,i}^{t+1}\}_{i=1}^{N_i}$ using (9).
 - 6: Draw the updated sample θ_j^{t+1} from $\{\theta_{j,i}^{t+1}\}_{i=1}^{N_i}$ randomly.
 - 7: **end for**
 - 8: **end for**
-

When the ensemble size is small, the posterior distribution may not be accurately captured. However, the ensemble can rapidly concentrate in regions of high posterior probability, which is particularly useful for multimodal distributions. Therefore, in our paper, instead of using ILUES directly as a sampler for the posterior, we employ it as an efficient generator of training data. We will describe it in more detail in Section 4.

3.3. MCMC with the Gaussian mixture proposal

Through iterative sampling and probabilistic transitions, the MCMC algorithm [35] allows us to generate samples from the target distribution $P(\theta)$. Starting from an initial point θ^0 , at iteration $t-1$, MCMC generates a candidate point θ^* from the proposal distribution $Q(\theta^*|\theta^{t-1})$. The candidate is then accepted with the probability

$$\alpha(\theta^*, \theta^{t-1}) = \min \left\{ 1, \frac{P(\theta^*)}{Q(\theta^*|\theta^{t-1})} \cdot \frac{Q(\theta^{t-1}|\theta^*)}{P(\theta^{t-1})} \right\}.$$

If θ^* is accepted, the new sample θ^t is updated as $\theta^t = \theta^*$; otherwise, the current sample is retained, i.e., $\theta^t = \theta^{t-1}$. A popular choice for the proposal distribution is the Gaussian distribution [36], which is symmetric, meaning that $Q(\theta^*|\theta^{t-1}) = Q(\theta^{t-1}|\theta^*)$. If the covariance of the proposal is small, the Markov chain randomly walks in a small parameter region. Conversely, if the covariance is too large, most candidate samples are likely to be rejected.

When the posterior distribution is multimodal, one can adopt a Gaussian mixture distribution as the proposal distribution when using MCMC to generate a large number of samples from the approximate posterior distribution $p_n(\theta)$ [37]. A Gaussian mixture (GM) distribution is a superposition of K different multivariate Gaussian components and is defined as

$$q(\theta) = \sum_{j=1}^K w_j \mathcal{N}(\theta|\mu_j, \Sigma_j),$$

where $w_j \geq 0$ are the mixture weights satisfying $\sum_{j=1}^K w_j = 1$.

Suppose that the GM proposal at iteration $t - 1$ is characterized by the parameters $\{w_j^{t-1}, \mu_j^{t-1}, \Sigma_j^{t-1}\}_{j=1}^K$. Then the proposal distribution at iteration $t - 1$ is given by

$$q(\theta|\theta^{t-1}) = \sum_{j=1}^K w_j^{t-1} \mathcal{N}(\theta|\mu_j, \Sigma_j^{t-1}). \quad (10)$$

Assume that the current sample θ^{t-1} belongs to mode j . Denote by m_j^{t-1} the number of samples previously assigned to mode j . Draw a candidate sample θ^t from the proposal distribution (10). Suppose that θ^t is assigned to mode i . Then the GM parameters can be updated as follows:

$$m_i^t = m_i^{t-1} + 1, \quad m_j^t = m_j^{t-1}, \quad j \neq i, \quad (11)$$

$$\mu_i^t = \frac{1}{m_i^t} \theta^t + \frac{m_i^{t-1} - 1}{m_i^t} \mu_i^{t-1}, \quad \mu_j^t = \mu_j^{t-1}, \quad j \neq i, \quad (12)$$

$$w_j^t = \frac{m_j}{t}, \quad j = 1, \dots, K, \quad (13)$$

$$\Sigma_i^t = \frac{1}{m_i^t} \left(\frac{(\theta^t - \mu_i^{t-1})(\theta^t - \mu_i^{t-1})^T}{m_i^{t-1}} + \epsilon \mathbf{I} \right) + \frac{m_i^{t-1} - 2}{m_i^t - 1} \Sigma_i^{t-1},$$

$$\Sigma_j^t = \Sigma_j^{t-1}, \quad j \neq i, \quad (14)$$

where $\epsilon > 0$ is a small number ensuring that the covariance matrix Σ_i^t remains positive definite [38], and \mathbf{I} denotes the identity matrix of appropriate dimension. For the target distribution $p_n(\theta) \propto \exp(\hat{f}_{n-1}(\theta))p_{n-1}(\theta)$, the acceptance probability is given by

$$\alpha(\theta^*, \theta^{t-1}) = \min \left\{ 1, \frac{\exp(\hat{f}_{n-1}(\theta^*))p_{n-1}(\theta^*)}{q(\theta^*|\theta^{t-1})} \cdot \frac{q(\theta^{t-1}|\theta^*)}{\exp(\hat{f}_{n-1}(\theta^{t-1}))p_{n-1}(\theta^{t-1})} \right\}. \quad (15)$$

To summarize, the procedure for the adaptive Metropolis MCMC with a Gaussian mixture proposal is as follows. The algorithm begins with an initial state θ^0 and an initial proposal distribution defined by the initial parameters of the Gaussian mixture model. At the t -th step, a candidate state θ^* is first generated from the current proposal $q(\theta^* | \theta^{t-1})$ in (10). The candidate state is then accepted with the acceptance probability $\alpha(\theta^*, \theta^{t-1})$ in (15). Once the new state θ^* is accepted, the parameters defining the Gaussian mixture model are updated using (11)-(14). The algorithm is summarized in Algorithm 3.

Algorithm 3 Adaptive Metropolis MCMC with Gaussian Mixture Proposal

Input: Length of the Markov chain N , initial parameters for the Gaussian mixture distribution $\{w_k^0, \mu_k^0, \Sigma_k^0\}$ and K .

Output: Samples $\{\theta_i\}_{i=1}^N$.

- 1: Generate the initial state θ^0 from the prior $\pi_{prior}(\theta)$.
 - 2: **for** $t = 1, \dots, N$ **do**
 - 3: Sample $\theta^* \sim q(\theta^*|\theta^{t-1})$ (the proposal distribution defined in (10))
 - 4: Compute the acceptance probability $\alpha(\theta^*, \theta^{t-1})$ using equation (15) with the proposal distribution (10).
 - 5: Sample z from a uniform distribution $\mathcal{U}(0, 1)$.
 - 6: **if** $\alpha(\theta^*, \theta^{t-1}) \geq z$ **then**
 - 7: Set $\theta^t = \theta^*$.
 - 8: **else**
 - 9: Set $\theta^t = \theta^{t-1}$.
 - 10: **end if**
 - 11: Update the parameters of the Gaussian mixture proposal $\{m_k^t, w_k^t, \mu_k^t, \Sigma_k^t\}$ for $k = 1, \dots, K$ using (11)-(14).
 - 12: **end for**
-

4. Our method: ILUES-based adaptive Gaussian process regression (ILUES-AGPR)

Now, we are ready to present our method, the ILUES-based adaptive Gaussian process regression (ILUES-AGPR), to solve Bayesian inverse problems with multimodal posterior distributions. As shown in (4), the unnormalized posterior density $\tilde{\pi}(\theta | \mathbf{d}_{obs})$ can be expressed as the product of $\exp(f(\theta))$ and an auxiliary distribution $p(\theta)$. Using $p(\theta)$, we construct a GP surrogate model $\hat{f}(\theta)$ to approximate $f(\theta)$. Starting from an initial density $p_0(\theta)$, we then iteratively update the GP surrogate $\hat{f}_n(\theta)$ and the approximate posterior $p_n(\theta)$ using (6) and (7), respectively, until $p_n(\theta)$ converges or the maximum number of iterations is reached.

However, constructing surrogate models solely based on the prior distribution can be inefficient when the posterior deviates significantly from the prior. Ideally, the surrogate model should be trained using samples drawn from the posterior distribution. However, this is impractical because the posterior is not available in advance. To address this challenge, we employ the ILUES method to adaptively generate informative training data concentrated in regions of high posterior density. In particular, when the ensemble size is small, ILUES tends to concentrate samples near the primary modes of the true posterior, even if the distribution of these points does not fully match the posterior.

Specifically, we run the ILUES algorithm shown in Algorithm 2 with N_e ensemble members for n_0 iterations, producing $N_e \times n_0$ parametermodel evaluation pairs $\mathbf{Z} = \{(\theta_j^n, \tilde{\pi}(\theta_j^n | \mathbf{d}_{obs})), j = 1, \dots, N_e, n = 1, \dots, n_0\}$. We then approximate the initial auxiliary distribution $p_0(\theta)$ using the last ensemble $\mathbf{E}_0 = \{\theta_j^{n_0}\}_{j=1}^{N_e}$ and denote the estimated probability density function as $\hat{p}_0(\theta)$. The initial training dataset for GP modeling is $\mathbf{S}_0 = \{(\theta_j^n, f_0(\theta_j^n)), j = 1, \dots, N_e, n = 1, \dots, n_0\}$, where $f_0(\theta)$ is defined in (6). Next, we construct the initial GP surrogate $\hat{f}_0(\theta)$ using \mathbf{S}_0 and $\hat{p}_0(\theta)$. Meanwhile, we apply K -means clustering to \mathbf{E}_0 to obtain the initial Gaussian mixture proposal, which is fully characterized by parameters $\{w_j, \mu_j, \Sigma_j\}_{j=1}^K$.

Algorithm 4 ILUES-based Adaptive Gaussian Process Regression (ILUES-AGPR)

Input: Initial number of iterations n_0 , ensemble size N_e for ILUES, forward model $\mathcal{G}(\theta)$, observational data \mathbf{d}_{obs} , maximum number of iterations N^{\max} for the overall algorithm, KL divergence threshold δ_{KL} , and maximum consecutive iterations N_{KL}^{\max} .

Output: The approximated posterior distribution $p_n(\theta)$.

- 1: Let $n_{KL} = 0$. Draw an initial archive $\mathbf{Z} = \{(\theta_j^n, \tilde{\pi}(\theta_j^n | \mathbf{d}_{obs}))\}$, $j = 1, \dots, N_e$, $n = 1, \dots, n_0$ using Algorithm 2, with n_0 iterations and the prior distribution $\pi_{prior}(\theta)$. Denote by $\mathbf{E}_0 = \{\theta_j^{n_0}\}_{j=1, \dots, N_e}$ the ensemble samples.
 - 2: Estimate the PDF for $p_0(\theta)$ using the last ensemble samples \mathbf{E}_0 , and denote it as $\hat{p}_0(\theta)$.
 - 3: Construct the initial training dataset $\mathbf{S}_0 = \{(\theta_j, f_0(\theta_j))\}$, $j = 1, \dots, N_e n_0$ with f_0 defined in (6).
 - 4: Build the GP surrogate model $\hat{f}_0(\theta)$ using $\hat{p}_0(\theta)$ and \mathbf{S}_0 .
 - 5: Obtain the initial parameters for the Gaussian mixture proposal using the K -means method: K and $\{\mu_k, \Sigma_k\}_{k=1}^K$.
 - 6: **for** $n = 1, \dots, N^{\max}$ **do**
 - 7: Draw M samples from the target density $p_n(\theta) \propto \exp(\hat{f}_{n-1}(\theta))\hat{p}_{n-1}(\theta)$ using MCMC with the Gaussian mixture proposal (see Algorithm 3), yielding samples A_n .
 - 8: Obtain an estimated probability density function (PDF) \hat{p}_n of $p_n(\theta)$ from samples A_n .
 - 9: Compute the KL divergence: $D_{KL}(\hat{p}_{n-1}, \hat{p}_n)$.
 - 10: **if** $D_{KL}(\hat{p}_{n-1}, \hat{p}_n) \leq \delta_{KL}$ **then**
 - 11: $n_{KL} = n_{KL} + 1$.
 - 12: **else**
 - 13: Reset $n_{KL} = 0$.
 - 14: **end if**
 - 15: **if** $n_{KL} = N_{KL}^{\max}$ **then**
 - 16: Terminate the for loop.
 - 17: **end if**
 - 18: Run one ILUES update iteration via (9) to obtain N_e new design points $\{\theta_j^{n+n_0}, j = 1, \dots, N_e\}$.
 - 19: Augment \mathbf{Z} with $\{\theta_j^{n+n_0}, \tilde{\pi}(\theta_j^{n+n_0} | \mathbf{d}_{obs})\}_{j=1, \dots, N_e}$ and update the training dataset to $\mathbf{S}_{n+1} = \{(\theta_j^{n+n_0}, f_n(\theta_j^{n+n_0}))\}$, $j = 1, \dots, N_e$.
 - 20: Construct the updated GP surrogate model $\hat{f}_n(\theta)$ with $\hat{p}_n(\theta)$ and the training dataset \mathbf{S}_{n+1} .
 - 21: Obtain the updated parameters for the GM proposal using the K -means method: K and $\{\mu_k, \Sigma_k\}_{k=1}^K$.
 - 22: **end for**
-

At iteration $n \geq 1$, given the current prior distribution $\hat{p}_{n-1}(\theta)$ and GP surrogate $\hat{f}_{n-1}(\theta)$, we draw M samples from the target density $p_n(\theta) \propto \exp(\hat{f}_{n-1}(\theta))\hat{p}_{n-1}(\theta)$ using MCMC with the GM proposal yielding samples A_n . We then approximate $p_n(\theta)$ by $\hat{p}_n(\theta)$ using the samples A_n and kernel density estimation. Next, we check the termination condition. We compute the KL divergence between the current PDF \hat{p}_n and the previous \hat{p}_{n-1} . If the divergence is smaller than the threshold δ_{KL} in N_{KL}^{\max} consecutive iterations the algorithm terminates. Otherwise, we perform one ILUES iteration to obtain $\mathbf{E}_{n+1} = \{\theta_j^{n+n_0}\}_{j=1,\dots,N_e}$. Finally, we augment \mathbf{Z} with $\{(\theta_j^{n+n_0}, \tilde{\boldsymbol{\pi}}(\theta_j^{n+n_0}|\mathbf{d}_{obs}))\}$, $j = 1, \dots, N_e$, and update the training dataset to

$$\mathbf{S}_{n+1} = \{(\theta_j^{n+n_0}, f_n(\theta_j^{n+n_0}))\}, j = 1, \dots, N_e$$

Our method is summarized in Algorithm 4.

5. Numerical examples

In this section, we will evaluate the performance of our proposed algorithm using two examples. All numerical experiments were conducted using MATLAB R2024a on a Windows 11 workstation with a 12-core CPU.

5.1. Example 1: contamination source identification

Consider the contaminant source inversion problem in a two-dimensional domain, where the goal is to infer the contaminant source based on a set of observations. The forward model is described by a parabolic equation:

$$\begin{aligned} \frac{\partial u(\mathbf{x}, t)}{\partial t} &= D\Delta u(\mathbf{x}, t), \quad \mathbf{x} \in \Omega = [-1, 1]^2, \quad t \in [0, \infty), \\ u(\mathbf{x}, t) &= 0, \quad \mathbf{x} \in \partial\Omega, \\ u(\mathbf{x}, 0) &= \frac{M}{2\pi h^2} \exp\left(\frac{-\|\boldsymbol{\xi} - \mathbf{x}\|^2}{2h^2}\right), \end{aligned} \tag{16}$$

where D is the diffusion coefficient, M is the total amount of released contaminant, and h is the radius of concentration source. We assume that D , M , and h are known parameters and are set to be 1, 15, and 0.1, respectively. The field $u(\mathbf{x}, t)$ represents the concentration of the contaminant, and $\boldsymbol{\xi}$ denotes the location of the contaminant.

In this example, the location of source, $\boldsymbol{\xi}$, is unknown and is treated as the inference parameter of interest. We set the prior as a uniform distribution $\boldsymbol{\xi} \sim \mathcal{U}([-1, 1]^2)$. The true value is set to $\boldsymbol{\xi} = (\xi_1, \xi_2) = (-0.5, 0.5)$. The observational data, \mathbf{d}_{obs} , are collected at the locations $(-0.4, -0.4)$ and $(0, 0.4)$ at time $t = 0.04$. We assume that the observations are contaminated by zero-mean Gaussian noise, whose standard deviation is set to 5% of the observed value. We use the finite difference method to solve the forward model (16) with a uniform mesh, where $\Delta x = 0.025$ and $\Delta t = 1.25 \times 10^{-4}$. The analytical form of the posterior distribution is not available. Therefore, we use the DREAM-KZS [17] algorithm with 8 parallel Markov chains with 2×10^5 iterations to generate the *true* posterior distribution. The DREAM-KZS implementation is available at https://github.com/zirandaode/DREAM_KZS. The posterior distribution obtained by DREAM-KZS for this example and the corresponding marginal probability density functions are shown in Figure 1. As seen, the distribution is multimodal. One mode corresponds to the true solution, while the other mode remains unknown.

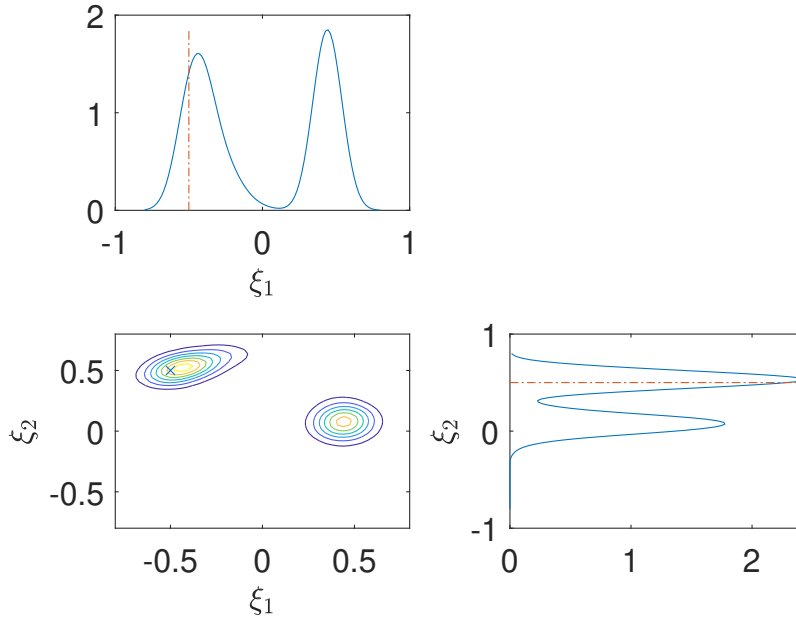


Figure 1: Joint posterior distribution for Example 1 and its marginal probability density functions.

We apply the proposed ILUES-AGPR method to this example and compare it with other approaches. Specifically, we use the ILUES algorithm to generate the initial archive $\mathbf{Z} = \{(\xi_j^t, \tilde{\pi}(\xi_j^t | \mathbf{d}_{obs})), j = 1, \dots, N_e, t = 1, \dots, t_0\}$, where the forward model is defined in (16), the ensemble size is set to $N_e = 80$, the number of initial iterations is $n_0 = 1$, and a uniform prior distribution is assumed. Using the ensemble samples, we perform kernel density estimation with the MATLAB package **kde** to approximate the initial PDF, $\hat{p}_0(\xi)$. The package is available at <https://ics.uci.edu/~ihler/code/kde.html>. Next, we apply the K -means method [39] to cluster the ensemble data points. Figure 2(a) shows the generated samples and the corresponding estimated PDF. Compared with the true posterior distribution shown in Figure 1, we observe that even with only one iteration, the ILUES algorithm successfully identified regions of high posterior probability, providing a reliable initial approximation for $p_0(\xi)$. Figure 2(d) presents the clustering results, where dots in different colors represent distinct clusters, asterisks indicate the cluster means, and contours represent the estimated PDF based on the ensemble samples. The kernel function used in the GP regression is the squared exponential kernel, and its hyperparameters are automatically optimized using a gradient descent method.

In this example, we set the MCMC chain length (M in Algorithm 4) to 1×10^4 and use a burn-in rate of 20%. The adaptive sampling process is illustrated in panels (a)-(c) of Figure 2. The training data points shown in Figure 2(a) are sampled using ILUES with a single iteration. Panels (b) and (c) of Figure 2 show the estimated probability density functions $\hat{p}_1(\xi)$ and $\hat{p}_2(\xi)$ obtained from the MCMC samples. The corresponding acceptance rates are 48.06% and 48.60%, respectively, which fall within a desirable range. In addition, the KL divergence between $\hat{p}_0(\xi)$ and $\hat{p}_1(\xi)$ is 0.7232, while that between $\hat{p}_1(\xi)$ and $\hat{p}_2(\xi)$ is 0.0422, indicating that the proposed algorithm can converge rapidly. Panels (e) and (f) of Figure 2 present the ensemble samples with clustering information, where contours

denote the estimated probability density functions based on the ensemble samples at iterations $n = 1$ and $n = 2$, respectively. Compared with panels (b) and (c) of Figure 2, these results show that ILUES is capable of generating samples concentrated in regions of high posterior probability. However, when the ensemble size is small, the resulting probability density function estimates may be unreliable.

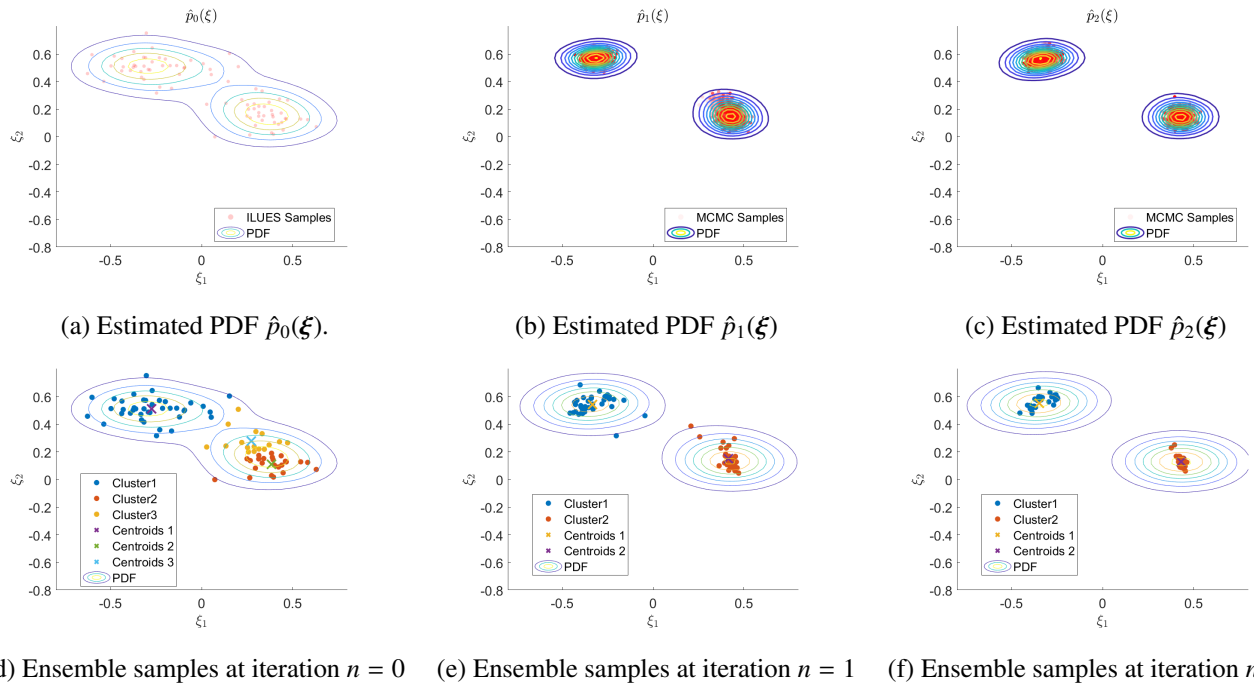


Figure 2: **Top row:** Approximated posterior distributions at iterations $n = 0, 1$, and 2 . Blue dots in (a) represent ILUES ensemble points, while (b) and (c) show MCMC-generated samples. **Bottom row:** Ensemble samples at iterations $n = 0, 1$, and 2 . Dots in different colors represent distinct clusters, X marks indicate cluster centroids, and contours display the estimated PDF based on the ensemble points.

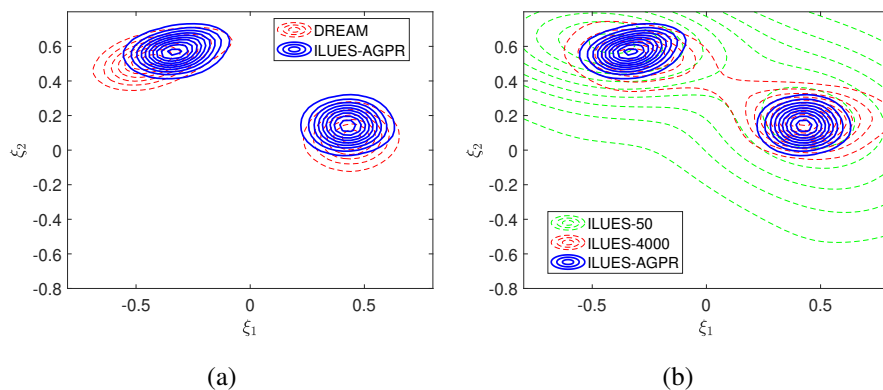


Figure 3: (a) Posterior probability density functions estimated by DREAM and ILUES-AGPR. (b) Posterior probability density functions estimated by ILUES-AGPR and ILUES with two ensemble sizes, $N_e = 50$ (ILUES-50) and $N_e = 4000$ (ILUES-4000).

We compare the posterior probability density functions obtained using DREAM, ILUES, and ILUES-AGPR. Specifically, Figure 3(a) compares the posterior probability density functions produced by DREAM and the proposed ILUES-AGPR method. As shown in Fig. 3(a), ILUES-AGPR successfully captures the same two dominant posterior

modes as DREAM, with comparable locations and shapes. This indicates that ILUES-AGPR is able to recover the intrinsic multimodal structure of the posterior distribution. Figure 3(b) presents the results obtained using ILUES with a single iteration for two ensemble sizes, $N_e = 50$ and $N_e = 4000$. Figure 3(b) further highlights the robustness of ILUES-AGPR with respect to ensemble size. When a small ensemble ($N_e = 50$) is used, ILUES produces severely distorted posterior distributions, indicating sample degeneracy and inadequate exploration of the parameter space. Increasing the ensemble size to $N_e = 4000$ still does not lead to a satisfactory posterior approximation, suggesting that simply enlarging the ensemble is insufficient. In contrast, ILUES-AGPR yields a stable and well-resolved multimodal posterior even with a moderate ensemble size, demonstrating its effectiveness in mitigating ensemble collapse and capturing the intrinsic multimodality of the inverse problem.

Method	Mean	Median	Standard Deviation
ILUES-50	0.24	0.23	0.02
ILUES-4000	31.49	31.50	0.57
ILUES-AGPR	45.28	45.18	0.61
DREAM	425.53	426.02	19.16

Table 1: Comparison of the running time (in seconds) for four methods.

Furthermore, Table 1 compares the computational efficiency of the four methods by reporting their mean and median running times (in seconds) based on 100 independent runs. The results show that ILUES is the fastest, ILUES-AGPR is marginally slower than ILUES-4000, and DREAM is the most computationally expensive. However, as illustrated in Fig. 3(b), the fastest method, ILUES-50, yields unsatisfactory estimation accuracy for this problem. Increasing the ensemble size to 4000 (ILUES-4000) does not lead to substantial performance gains, indicating limited accuracy improvements from simply enlarging the ensemble. In contrast, ILUES-AGPR achieves significantly better estimation accuracy than ILUES-4000 while maintaining a comparable computational cost. DREAM provides more reliable posterior estimates due to its Markov chain Monte Carlo sampling mechanism, it is nearly ten times slower than ILUES-AGPR (425.53 vs. 45.28 seconds). This highlights ILUES-AGPR as the most favorable trade-off between efficiency and accuracy. These findings establish our proposed method, ILUES-AGPR, as the most favorable trade-off between computational efficiency and estimation accuracy.

5.2. Example 2: contamination source location and strength identification

In the second example, we consider a Poisson equation with mixed boundary conditions:

$$\begin{aligned}
 -\nabla \cdot (a(\mathbf{x})\nabla u(\mathbf{x})) &= f(\mathbf{x}), & \mathbf{x} \in D = [0, 1]^2, \\
 u(0, y) &= 0, & u(1, y) = 0,
 \end{aligned}
 \tag{17}$$

where the remaining two boundaries are subject to no-flow (Neumann) boundary conditions. The coefficient $a(\mathbf{x})$ denotes the permeability field, which is assumed to be uniform, i.e., $a(\mathbf{x}) = 0.2$. The source term is given by

$$f(\mathbf{x}) = \frac{|s|}{2\pi h^2} \exp\left(-\frac{\|\mathbf{x} - \boldsymbol{\xi}\|^2}{2h^2}\right),
 \tag{18}$$

where $\boldsymbol{\xi} = (\xi_1, \xi_2)$ is the location of the source, h and s represent the width and strength of the source, respectively. In this example, we assume that the source width h is known and fixed at 0.05. Both the source strength s and the source location $\boldsymbol{\xi}$ are treated as unknown parameters of interest. Accordingly, the unknown parameter vector is defined as $\boldsymbol{\theta} = (\xi_1, \xi_2, s)$.

Sensor measurements are defined through an observation operator \mathcal{O} acting on the PDE solution, i.e.,

$$\mathbf{d}_{obs} = \mathcal{O}(u(\mathbf{x}; \boldsymbol{\theta})) + \eta,$$

where $\mathcal{O}(u) = [u(\mathbf{x}^{(1)}), u(\mathbf{x}^{(2)}), \dots, u(\mathbf{x}^{(\bar{D})})]$ corresponds to pointwise sampling of the solution at \bar{D} sensor locations $\{\mathbf{x}^{(i)}\}_{i=1}^{\bar{D}}$. In this example, the synthetic PDE solution u is generated by solving the forward model (17) on a uniform 32×32 mesh using a finite element solver [40], the sensors are distributed on a uniform 3×3 grid covering the region $[0.3, 0.7] \times [0.3, 0.7]$. The true source location and strength are set to $\boldsymbol{\xi} = (0.6, 0.6)$ and $s = 1$, respectively. Measurement noise is assumed to be independent distributed Gaussian noise with zero mean and a standard deviation equal to 5% of the observed value. The prior distribution of s is taken as uniform on $\mathcal{U}(-2, 2)$, while the prior for the source location $\boldsymbol{\xi}$ is assumed to be uniform over the domain D .

The source function in (18) is symmetric with respect to s , leading to a bimodal posterior distribution for s , with modes centered at $s = 1$ and $s = -1$. In contrast, the marginal posterior distribution of the source location $\boldsymbol{\xi}$ is unimodal. To generate the *true* posterior distribution, we employ the DREAM-KZS algorithm with eight parallel Markov chains and 2×10^5 iterations. The corresponding one-dimensional (1D) and two-dimensional (2D) marginal probability density functions are shown in Figure 4.

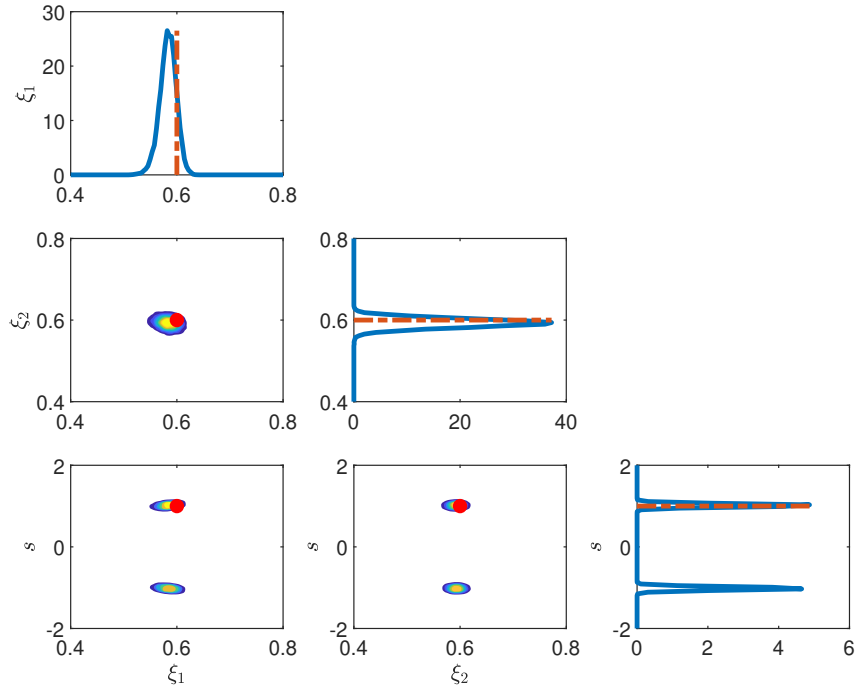


Figure 4: One-dimensional (1D) and two-dimensional (2D) marginal posterior probability density functions obtained using DREAM-KZS for Example 2.

We use this example to illustrate the effect of the ensemble size N_e . In the ILUES step of our method ILUES-AGPR, we consider two cases with $N_e = 80$ and $N_e = 150$, respectively, for which the forward model is evaluated separately at each iteration. In the following subsection, these two settings are referred to as **Ne80** and **Ne150**, respectively. In both cases, the number of initial iterations is set to $n_0 = 4$.

For both the **Ne80** and **Ne150** cases, the prior samples are uniformly distributed over the parameter space, as shown in panels (a) and (d) of Figure 5, respectively. After n_0 iterations and clustering, the resulting samples are shown in panels (b) and (e), where different colors denote different clusters. The corresponding approximate distributions are presented in panels (c) and (f), respectively. These results indicate that, although the ILUES step captures both modes in each case, the distribution in the **Ne80** case tends to collapse toward a single mode.

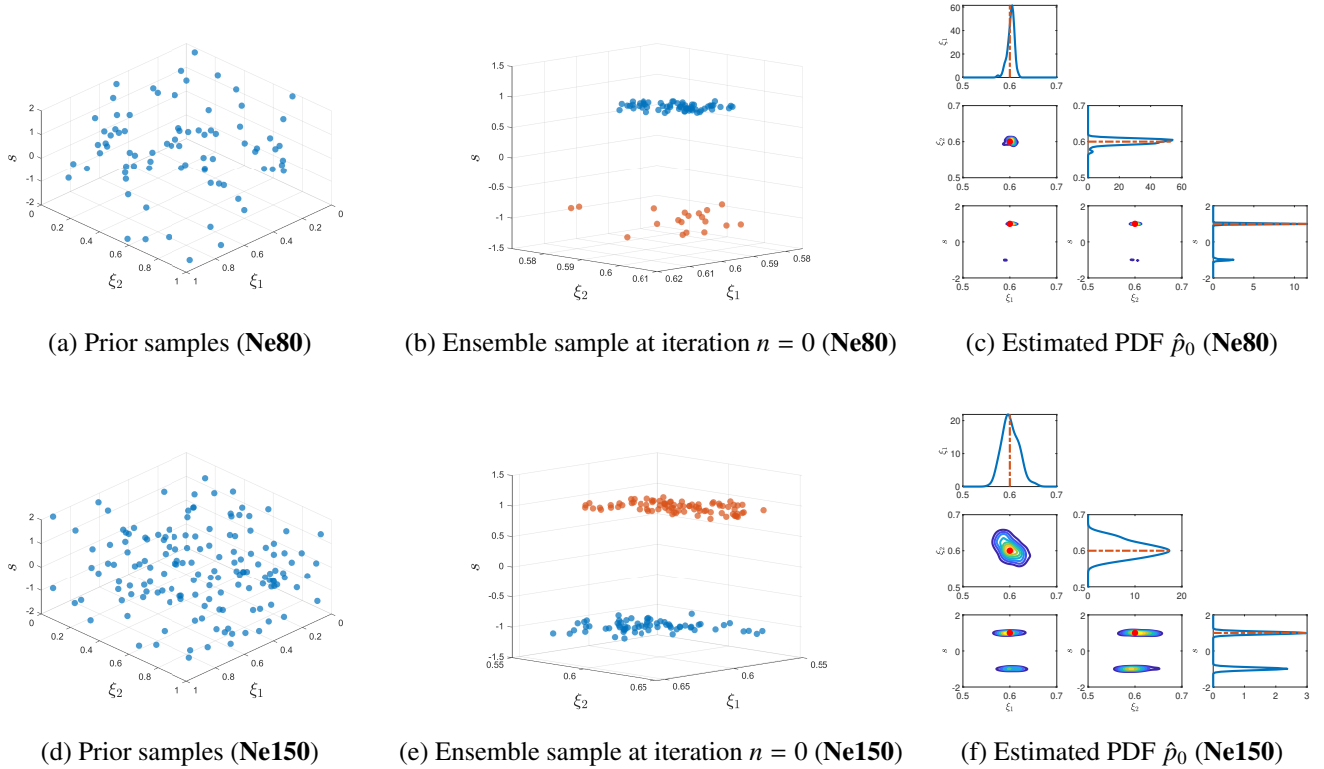


Figure 5: **Top row:** ILUES step for the **Ne80** case. (a) Prior samples (blue dots). (b) Ensemble samples after n_0 iterations with clustering, where different colors indicate different clusters. (c) Corresponding 1D and 2D marginal estimated probability density function (PDF), \hat{p}_0 . **Bottom row:** ILUES step for the **Ne150** case. (d) Prior samples (blue dots). (e) Ensemble samples after n_0 iterations with clustering, with colors representing clusters. (f) Corresponding 1D and 2D marginal estimated PDF, \hat{p}_0 .

In this example, we use the same Gaussian process settings as in Example 1. We set the MCMC chain length (M in Algorithm 4) to 4×10^4 and use a burn-in rate of 30%. The maximum number of iterations N^{\max} is set to 6, the KL-divergence threshold δ_{KL} is set to 0.05, and the maximum number of consecutive iterations N_{KL}^{\max} is set to 2. In the **Ne80** case, the algorithm terminates at $n = 3$. The KL divergences $D_{\text{KL}}(\hat{p}_{n-1}, \hat{p}_n)$ for $n = 0, 1, 2, 3$ are 0.45, 0.16, 0, and 0, respectively. The corresponding MCMC acceptance rates for $n = 1, 2, 3$ are 26.70%, 28.61%, and 26.70%. In the **Ne150** case, the algorithm also terminates at $n = 3$. The KL divergences for $n = 0, 1, 2, 3$ are 0.37,

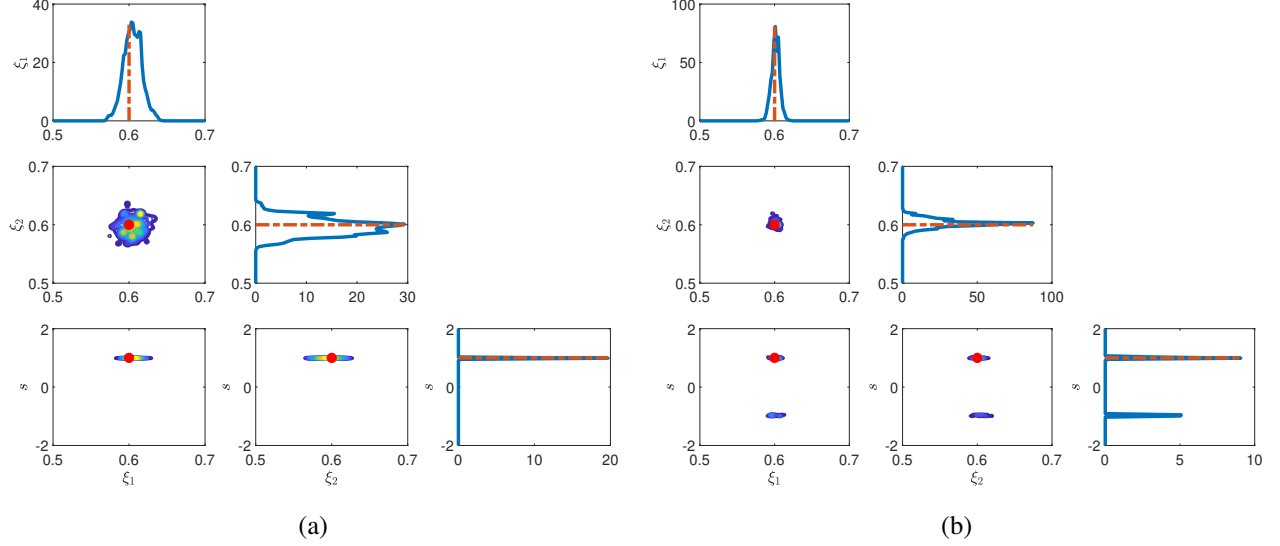


Figure 6: Estimated 1D and 2D marginal posterior probability density functions for the **Ne80** and **Ne150** cases. (a): **Ne80**; (b): **Ne150** case.

0.19, 0.04, and 0.012, respectively, with MCMC acceptance rates of 27.90%, 24.29%, and 25.20% for $n = 1, 2, 3$, respectively. Overall, the convergence behavior and MCMC performance are nearly identical in both cases. However, the computational cost differs: the total runtime is 103 seconds for the **Ne80** case and 125 seconds for the **Ne150** case. Owing to the smaller ensemble size, the **Ne80** configuration is slightly more efficient.

Figure 6 shows the marginal posterior density functions of θ along with the contours of the corresponding 2-dimensional marginal PDF. In Panel (a) of Figure 6, the final posterior for the **Ne80** case is trapped in a single mode, failing to capture the multimodal distribution. In contrast, Panel (b) shows that the **Ne150** case successfully captures both modes.

These results highlight the importance of choosing an appropriate ensemble size N_e . A small N_e can lead to mode collapse, whereas a large N_e may reduce computational efficiency. The impact of N_e on the overall algorithm primarily arises in two aspects. First, the quality of the prior distribution generated by ILUES can vary significantly. Second, the number of training points available for the GP surrogate changes accordingly. With a smaller training dataset, the GP surrogate may perform suboptimally, resulting in *jitter* in the posterior distribution generated by MCMC, as observed in Panel (a) of Figure 6.

6. Conclusion

In this paper, we address the challenge of efficiently approximating multimodal posterior distributions arising in Bayesian inverse problems. We reviewed the formulation of Bayesian inverse problems and relevant existing methodologies, including adaptive Gaussian process surrogates and the ILUES method. Building on these foundations, we proposed a new approach for efficiently sampling from multimodal posterior distributions. Numerical examples demonstrate that the effectiveness and overall efficiency of the proposed ILUES-AGPR algorithm.

References

- [1] A. Tarantola, *Inverse problem theory and methods for model parameter estimation*, Society for Industrial and Applied Mathematics, 2005.
- [2] J. K. Kruschke, *Bayesian data analysis*, *Wiley Interdisciplinary Reviews: Cognitive Science* 1 (5) (2010) 658–676.
- [3] M. Asch, M. Bocquet, M. Nodet, *Data Assimilation: Methods, Algorithms, and Applications*, SIAM, 2016.
- [4] F. Rizzi, M. Salloum, Y. Marzouk, R.-G. Xu, M. Falk, T. Weihs, G. Fritz, O. M. Knio, Bayesian inference of atomic diffusivity in a binary Ni/Al system based on molecular dynamics, *Multiscale Modeling & Simulation* 9 (1) (2011) 486–512.
- [5] J. Kaipio, E. Somersalo, *Statistical and Computational Inverse Problems*, Vol. 160, Springer Science & Business Media, 2005.
- [6] C. Andrieu, N. De Freitas, A. Doucet, M. I. Jordan, An introduction to MCMC for machine learning, *Machine learning* 50 (2003) 5–43.
- [7] T. Cui, K. J. Law, Y. M. Marzouk, Dimension-independent likelihood-informed MCMC, *Journal of Computational Physics* 304 (2016) 109–137.
- [8] A. Beskos, K. Kamatani, MCMC algorithms for posteriors on matrix spaces, *Journal of Computational and Graphical Statistics* 31 (3) (2022) 721–738.
- [9] H. Dai, M. Pollock, G. O. Roberts, Bayesian fusion: Scalable unification of distributed statistical analyses, *Journal of the Royal Statistical Society, Series B* 85 (1) (2023) 84–107.
- [10] Z. Xu, Q. Liao, J. Li, Domain-decomposed bayesian inversion based on local karhunen-loève expansions, *Journal of Computational Physics* (2024) 112856.
- [11] Z. Xu, Y. Xia, Q. Liao, A domain-decomposed VAE method for Bayesian inverse problems, *International Journal for Uncertainty Quantification* 14 (2024) 67–95.
- [12] J. Latz, J. P. Madrigal-Cianci, F. Nobile, R. Tempone, Generalized parallel tempering on Bayesian inverse problems, *Statistics and Computing* 31 (5) (2021) 67.
- [13] G. Lin, Y. Wang, Z. Zhang, Multi-variance replica exchange SGMCMC for inverse and forward problems via Bayesian PINN, *Journal of Computational Physics* 460 (2022) 111173.
- [14] M. K. Łącki, B. Miasojedow, State-dependent swap strategies and automatic reduction of number of temperatures in adaptive parallel tempering algorithm, *Statistics and Computing* 26 (5) (2016) 951–964.

- [15] J. A. Vrugt, C. Ter Braak, C. Diks, B. A. Robinson, J. M. Hyman, D. Higdon, Accelerating markov chain monte carlo simulation by differential evolution with self-adaptive randomized subspace sampling, *International Journal of Nonlinear Sciences and Numerical Simulation* 10 (3) (2009) 273–290.
- [16] J. A. Vrugt, C. J. Ter Braak, M. P. Clark, J. M. Hyman, B. A. Robinson, Treatment of input uncertainty in hydrologic modeling: Doing hydrology backward with Markov chain Monte Carlo simulation, *Water Resources Research* 44 (12) (2008) W00B09.
- [17] J. Zhang, J. A. Vrugt, X. Shi, G. Lin, L. Wu, L. Zeng, Improving simulation efficiency of MCMC for inverse modeling of hydrologic systems with a kalman-inspired proposal distribution, *Water Resources Research* 56 (3) (2020) e2019WR025474.
- [18] I. Bilonis, N. Zabarar, B. A. Konomi, G. Lin, Multi-output separable gaussian process: Towards an efficient, fully bayesian paradigm for uncertainty quantification, *Journal of Computational Physics* 241 (2013) 212–239.
- [19] M. Seeger, Gaussian processes for machine learning, *International Journal of Neural Systems* 14 (02) (2004) 69–106.
- [20] H. Wang, J. Li, Adaptive Gaussian process approximation for Bayesian inference with expensive likelihood functions, *Neural Computation* 30 (11) (2018) 3072–3094.
- [21] Y. M. Marzouk, H. N. Najm, L. A. Rahn, Stochastic spectral methods for efficient Bayesian solution of inverse problems, *Journal of Computational Physics* 224 (2) (2007) 560–586.
- [22] J. Li, Y. M. Marzouk, Adaptive construction of surrogates for the Bayesian solution of inverse problems, *SIAM Journal on Scientific Computing* 36 (3) (2014) A1163–A1186.
- [23] J. Zhang, Q. Zheng, D. Chen, L. Wu, L. Zeng, Surrogate-based Bayesian inverse modeling of the hydrological system: An adaptive approach considering surrogate approximation error, *Water Resources Research* 56 (1) (2020) e2019WR025721.
- [24] Y. Xia, N. Zabarar, Bayesian multiscale deep generative model for the solution of high-dimensional inverse problems, *Journal of Computational Physics* 455 (2022) 111008.
- [25] Y. Zhu, N. Zabarar, Bayesian deep convolutional encoder–decoder networks for surrogate modeling and uncertainty quantification, *Journal of Computational Physics* 366 (2018) 415–447.
- [26] A. D. Davis, Y. Marzouk, A. Smith, N. Pillai, Rate-optimal refinement strategies for local approximation MCMC, *Statistics and Computing* 32 (4) (2022) 1–23.
- [27] P. R. Conrad, Y. M. Marzouk, N. S. Pillai, A. Smith, Accelerating asymptotically exact MCMC for computationally intensive models via local approximations, *Journal of the American Statistical Association* 111 (516) (2016) 1591–1607.

- [28] P. R. Conrad, A. D. Davis, Y. M. Marzouk, N. S. Pillai, A. Smith, Parallel local approximation MCMC for expensive models, *SIAM/ASA Journal on Uncertainty Quantification* 6 (1) (2018) 339–373.
- [29] J. Sacks, W. J. Welch, T. J. Mitchell, H. P. Wynn, Design and analysis of computer experiments, *Statistical Science* 4 (4) (1989) 409–423.
- [30] D. J. MacKay, Information-based objective functions for active data selection, *Neural Computation* 4 (4) (1992) 590–604.
- [31] P. J. Van Leeuwen, G. Evensen, Data assimilation and inverse methods in terms of a probabilistic formulation, *Monthly Weather Review* 124 (12) (1996) 2898–2913.
- [32] J.-A. Skjervheim, G. Evensen, J. Hove, J. G. Vabø, An ensemble smoother for assisted history matching, in: *SPE Reservoir Simulation Symposium*, The Woodlands, Texas, USA, OnePetro, 2011. doi:doi.org/10.2118/141929-MS.
- [33] A. A. Emerick, A. C. Reynolds, Ensemble smoother with multiple data assimilation, *Computers & Geosciences* 55 (2013) 3–15.
- [34] J. Zhang, G. Lin, W. Li, L. Wu, L. Zeng, An iterative local updating ensemble smoother for estimation and uncertainty assessment of hydrologic model parameters with multimodal distributions, *Water Resources Research* 54 (3) (2018) 1716–1733.
- [35] C. Robert, G. Casella, *Monte Carlo Statistical Methods*, Springer Science & Business Media, 2013.
- [36] W. K. Hastings, Monte Carlo sampling methods using Markov chains and their applications, *Biometrika* 57 (1) (1970) 97 – 109.
- [37] B. Che, Y. Chen, Z. Huan, D. Z. Huang, W. Wang, Stable derivative free Gaussian mixture variational inference for Bayesian inverse problems, *SIAM Journal on Scientific Computing* 47 (5) (2025) A2583–A2608.
- [38] H. Haario, E. Saksman, J. Tamminen, An adaptive Metropolis algorithm, *Bernoulli* 7 (2) (2001) 223–242.
- [39] S. D. Landtsheer, `kmeans_opt`, MATLAB Central File Exchange. Retrieved August 15, 2024. (2024). URL https://www.mathworks.com/matlabcentral/fileexchange/65823-kmeans_opt
- [40] H. Elman, D. Silvester, A. Wathen, *Finite Elements and Fast Iterative Solvers: with Applications in Incompressible Fluid Dynamics*, Oxford University Press, 2014.